Molecular Vision 2021; 27:206-220 <http://www.molvis.org/molvis/v27/206>
Received 1 September 2019 | Accepted 29 April 2021 | Published 1 May 2021

Synaptic changes and the response of microglia in a light-induced photoreceptor degeneration model

Sisi Xu,[1,2,3] Peijun Zhang,[1,2,3] Meng Zhang,[1,2,3] Xin Wang,[1,2,3] Gang Li,[4] Gezhi Xu,[1,2,3] Yingqin Ni[1,2,3]

(The first two authors contributed equally to the work.)

[1]Department of Ophthalmology, Eye & ENT Hospital, Fudan University, Shanghai, China; [2]Shanghai Key Laboratory of Visual Impairment and Restoration, Fudan University, Shanghai, China; [3]Key NHC Key Laboratory of Myopia (Fudan University); Laboratory of Myopia, Chinese Academy of Medical Sciences, Shanghai, China; [4]Research Center, Eye & ENT Hospital of Fudan University, Shanghai, China

Purpose: To explore synaptic changes and the response of microglia in a light-induced photoreceptor degeneration model.

Methods: Sprague-Dawley rats were euthanized 1 h, 1 day, 3 days, 7 days, and 14 days after being exposed to intense blue light for 24 h. Hematoxylin and eosin (H&E) and terminal deoxynucleotidyl transferase dUTP nick-end labeling (TUNEL) staining were used to evaluate changes in the outer nuclear layer (ONL). Transmission electron microscopy (TEM) was applied to observe the ultrastructural changes in the synapses between the photoreceptors and second-order neurons. Western blotting was conducted to evaluate specific proteins, including postsynaptic density-95 (PSD-95), metabotropic glutamate receptor 6 (mGluR6), synapsin I, and synaptophysin. Immunofluorescence of CD11b and PKC-α or mGluR6 was used to explore the spatial relationships between microglial processes and synaptic elements. Immuno-electron microscopy of PSD-95 was performed to further confirm its engulfment of synaptic materials.

Results: H&E and TUNEL staining showed that the thickness of the ONL decreased markedly, and the number of apoptotic photoreceptors peaked at day 1. TEM revealed darkened photoreceptor terminals and that ribbons of them were floating in the cytoplasm, coinciding with the downregulation of PSD-95 and mGluR6. Downstream synaptic protein synapsin I and synaptophysin exhibited upregulation in the inner plexiform layer. Activated microglia migrated to the outer retina, and their processes were found in close proximity to synapses in the outer plexiform layer under light and electron microscopy levels. Double immunostaining of CD11b and mGluR6 showed colocalization. PSD-95-immuno-reactive electron-dense materials were observed inside the microglia suggesting engulfment of synaptic components.

Conclusions: The study showed that there are early synaptic impairment and late compensatory changes in downstream synapses in this photic injury model. Activated microglia touched and directly engulfed synaptic materials. Microglia may play a role or a partial role in synaptic changes.

Retinal degeneration diseases are a collection of diseases that can ultimately lead to irreversible visual impairment or even blindness [1]. Due to various pathogeneses, these diseases present in different forms with varying age of onset, degree of visual impairment, and accompaniment of other neurologic symptoms. However, loss of photoreceptors is the common final pathway [2]. In the past, it was believed that photoreceptor degeneration affected only the outer retina, leaving the inner retina relatively intact [3]. Recent literature has suggested that interneurons undergo a series of changes accompanying and after this process [4,5]. Modifications or loss of the synapses between the photoreceptors and interneurons may be an early and critical event [6,7].

Correspondence to: Yingqin Ni, Department of Ophthalmology, Shanghai Key Laboratory of Visual Impairment and Restoration, Eye & ENT Hospital, Fudan University, 83 Fenyang Road, Shanghai 200031, China; Phone: 021-64377134; FAX: 021-64376491; email: niniyingqin@126.com

Synapses, exquisite structures between two neurons or between a neuron and its effector, play a vital role in transferring information. The synapses in the retina are some of the most complex structures in the central nervous system (CNS) [8], because the information they transmit encodes, e.g., luminance, temporal or spatial resolution, and color. Pathological remodeling of synapses interferes with the processing of visual signals which may account for the limited therapeutic effect of photoreceptor transplantation and retinal prosthetic implantation [9,10].

Microglia, the major resident immune cells in the CNS, have been widely known to participate in the processes of tissue inflammation and clearance of cellular debris [11]. Recent studies have revealed the role of microglia in the maintenance of synaptic homeostasis by directly contacting synaptic elements [12,13]. During the postnatal development of the uninjured brain, engulfment and elimination of synapses by microglia are required for synaptic maturation

[14]. After depletion of microglia from the retina in transgenic mice, Wang et al. observed a pronounced declining b-wave on the electroretinogram and a breakdown of synaptic structural integrity in the outer plexiform layer (OPL) and the inner plexiform layer (IPL) [15]. This demonstrated the requirement for microglia in the maintenance of synapses in the healthy adult retina. In pathological situations, such as Alzheimer disease, microglia have been found to promote phagocytosis of synaptic structures, and this function could occur before amyloid deposition [16]. In experimental Parkinsonism, activated microglia selectively eliminate glutamatergic synapses [17]. At present, research on the effect of microglia on synapses has primarily come from studies of the brain or other fields [14,16,17]. However, little is known about the effect of microglia on synapses during retinal degeneration.

Therefore, the purpose of this study was to explore synaptic changes and the response of microglia in a light-induced photoreceptor degeneration model. The results showed that there are early synaptic impairments and late compensatory changes in downstream synapses in this photic injury model. Activated microglia touched and directly engulfed synaptic materials.

METHODS

Animals: All procedures were conducted in accordance with the ARVO statement for the Use of Animals in Ophthalmic and Vision Research. The study was approved by the Animal Ethics Committee of the Eye & ENT Hospital of Fudan University. One hundred and fourteen adult male Sprague-Dawley (SD) rats from SLAC Laboratories (Shanghai, China), each weighing 180 to 200 g, were maintained in a 12 h:12 h light-dark cycle with free access to food and water.

Model of light-induced retinal degeneration: The SD rats were randomly divided into light exposure and control groups. The control rats experienced 24 h dark adaptation and then were returned to the 12 h:12 h light-dark cycle. The rats in the light exposure group were dark adapted for 24 h, then separated in different cages, and exposed to 2,500 lux blue fluorescent light for 24 h. The rats then were returned to the normal 12 h:12 h light-dark cycle for 1 h, 1 day, 3 days, 7 days, or 14 days before further analysis.

Hematoxylin and eosin (H&E) staining: At different time points after light exposure, SD rats were euthanasia by an intraperitoneal injection of ketamine (200 mg/kg), mixed with xylazine (10 mg/kg). The eyes were enucleated and fixed in 4% paraformaldehyde. Four eyes were used for each time point. After immersion in 70% alcohol, paraffin-embedding and then sectioning (5 μm thick) were performed. Sections through the optic nerve head were collected and stained. Images were taken using a light microscope (Leica Microsystems, Bensheim, Germany). The thickness of the outer nuclear layer (ONL) and OPL was measured at 500 μm intervals starting at the optic papilla. The thickness was measured at 18 locations and the results were averaged.

Transmission electron microscopy (TEM): Four eyes were used for each time point. The eyes were rapidly removed and incised, and the retinas were taken out and fixed in 4% paraformaldehyde and 3% glutaraldehyde for at least 2 h at 4°C. After being rinsed in 0.1 M phosphate buffer three times (10 - 15 min each time), the tissues were postfixed in 1% osmium tetroxide for 2 h and washed three times in 0.1 M phosphate buffer. The tissues were dehydrated in a graded series of ethanol and transferred to acetone. The retinas were infiltrated with epon and were embedded in epon. Ultrathin sections (70 nm) were cut on an ultratome. They were collected on 200 mesh grids and analyzed under a JEM-1230 (JEOL Ltd., Tokyo, Japan) or a FEI Tecnai G2 Spirit TWIN (Eindhoven, the Netherlands) electron microscope at 80KV.

Western blotting: SD rats were euthanasia by an intraperitoneal injection of ketamine (200 mg/kg), mixed with xylazine (10 mg/kg) 1 hour, 1 day, 3 days, 7 days or 14 days after light exposure. Four retinas were used for each time point. Ultrasound was used to homogenize retinas. Equal amounts of proteins were loaded and separated using sodium dodecyl sulfate polyacrylamide gel electrophoresis (SDS-PAGE, Beyotime Biotechnology, Shanghai, China) and were then transferred to polyvinylidene fluoride (PVDF) membranes (Millipore, Billerica, MA). After 1 h blocking in 5% nonfat milk, the membranes were incubated overnight at 4°C with the following primary antibodies: post synaptic density-95 (PSD-95), metabotropic glutamate receptor 6 (mGluR6), Synapsin I, synaptophysin, β-actin, followed by the horseradish peroxidase-conjugated goat anti-rabbit (1:10000, Thermo Fisher Scientific) and goat anti-mouse (1:10000, Thermo Fisher Scientific) secondary antibody for 1 h. All primary antibodies used were listed in Table 1. The immunoblots were visualized with chemiluminescence (ECL Detection Reagent, Yeasen, Shanghai, China). The density of the signals was quantified using ImageJ and normalized against the loading controls. First, convert the type of images to 8-bit and subtract the background according to the actual situation. Then, set the unit of length to pixels and invert the pictures. Select the extent of the strip and measure the mean gray value.

Immunofluorescence: At 1 h, 1 day, 3 days, 7 days, or 14 days after light exposure, the eyes were enucleated and put into paraformaldehyde for 1 h at room temperature. Paraformaldehyde-fixed and optimal cutting temperature

compound-embedded retinas were sectioned at a thickness of 10 µm. Sections, cut through the optic papilla, were kept. The slides were incubated with blocking buffer (5% goat serum) at room temperature for 1 h. Incubation with the following primary antibodies was performed: mGluR6, synaptophysin, CD11b and mGluR6, CD11b and protein kinase C-α (PKC-α), CD11b, and CD68. Subsequently, the sections were washed three times with 0.01 M phosphate buffer saline (PBS, 1X; 155 mM NaCl, 3 mM Na_2HPO_4-$7H_2O$, 1 mM KH_2PO_4, pH 7.4) and incubated with Alexa 488-conjugated goat anti-mouse (1:1000, Thermo Fisher Scientific), Alexa 555-conjugated goat anti-rabbit (1:1000, Thermo Fisher Scientific) for 1 h. All primary antibodies used are listed in Table 1. All the slides were photographed using a confocal microscope (Leica TCS SP8). Regarding quantification of the staining intensity of synaptophysin in the IPL, all slides were stained and photographed at the same time at different time points. The photography parameters, such as exposure and brightness, were consistent. Pictures were analyzed using ImageJ. The boundary of the IPL was segmented, and the mean optical density was measured. Detailed software operation methods were uploaded as supplemental materials (Appendix 1). Six eyes were used for each time point. Regarding quantification of the number of microglia in the outer retina, CD11b-positive cells in the OPL, ONL, and subretinal space along the full length of the retinal cryosection were recorded. Six eyes were used for each time point. Terminal deoxynucleotidyl transferase dUTP nick-end labeling (TUNEL) staining was conducted using the Trevigen Apoptotic Cell System (TACS®) 2 TdT-Fluor in Situ Apoptosis Detection Kit (Trevigen, Gaithersburg, MD) according to the manufacturer's instructions

Immunoelectron microscopy (IEM): Two eyes were used for each time point. The eyes were placed in a fixative solution containing 4% paraformaldehyde and 0.3% glutaraldehyde for 2 h at 4 °C. They were then washed in 0.1 M phosphate buffer (PB) buffer, dehydrated in a graded ethanol series, and embedded in Epon. Ultrathin sections were cut and collected on 200 mesh nickel grids. The grids were placed on a droplet of 50 mM glycine for 30 min and then washed with double distilled water. After etching with 1% sodium periodate for 10 min, the grids were again washed with double distilled water. The grids were then floated upside down on a 20 µl drop of 5% bovine serum albumin (BSA) for 20 min. After blotting, the grids were placed on top of a 20 µl drop of the primary antibody PSD-95 (1:20, diluted in 1% BSA) for 24 h at 4 °C. After incubation with the primary antibody, the grids were washed 12 times (5 min each) on drops of 0.01 M PBS before a 20 min incubation on 20 µl of 1% BSA blocking buffer. They were then placed on 20 µl drops of 10 nm gold conjugated secondary antibody (1:50, Sigma-Aldrich) for 2 h at room temperature. Next, they were washed 12 times (5 min each) on drops of 0.01 M PBS and two times (2 min each) on drops of double distilled water to remove residual salt. Negative controls were treated in exactly the same way; however, no primary antibody was applied. Finally, the grids were allowed to dry at room temperature and imaged on a JEM-1230 (JEOL Ltd.) or a FEI Tecnai G2 Spirit TWIN (Eindhoven, the Netherlands) electron microscope at 80KV.

Statistical analysis: Experiments were repeated at least three times. Experimental data were analyzed with one-way analysis of variance (ANOVA) followed by Tukey's post hoc test. A p value of less than 0.05 was considered statistically significant.

Table 1. Primary antibodies used for Western Blot and immunofluorescence analysis.

Antibody	Company	Host	Catalogue#	Dilution Factor IF	Dilution Factor WB
PSD-95	Thermo Fisher Scientific (Waltham, MA)	Mouse	MA1–046	1:200	1:2000
mGluR6	Neuromics (Edina, MN)	Rabbit	RA13105	1:300	1:1000
Synapsin I	Merckmillipore (Billerica, MA)	Rabbit	AB1543P	-	1:16000
synaptophysin	Sigma-Aldrich (St. Louis, MO)	Mouse	S5768	1:1000	1:4000
β-actin	Santa Cruz Biotechnology (Santa Cruz, CA)	Mouse	sc-47778	-	1:1000
CD11b	Abcam (Cambridge, UK)	Mouse	ab1211	1:100	-
PKC-α	Abcam (Cambridge, UK)	Rabbit	ab32376	1:100	-
CD68	Abcam (Cambridge, UK)	Rabbit	ab125212	1:100	-

RESULTS

Light-induced photoreceptor degeneration: As shown in the H&E staining (Figure 1A–F), intense blue light exposure resulted in the progressive loss of photoreceptors. At day 14, only one to two lines of photoreceptors remained. Quantification of the thickness of the ONL is shown in Figure 1M. TUNEL staining was used to detect apoptotic cells. In the control retinas, positive staining was seldom observed (Figure 1G). At 1 h after light exposure, TUNEL-positive cells started to appear in the ONL (Figure 1H). At day 1 after light exposure, there were numerous TUNEL-positive cells scattered in the ONL, indicating apoptosis of the photoreceptors (Figure 1I). At day 3, there were only sporadic TUNEL-positive cells observed in the ONL (Figure 1J). As the degeneration progressed, the number of TUNEL-positive cells decreased (Figure 1K–L).

Impairment of the first synapses of the retina from early onset: Along with the attenuation of the ONL, the OPL, a layer normally occupied by synapses between the photoreceptors and bipolar cells, exhibited a gradual decrease (Figure 1N, Figure 2A,B). To further examine the ultrastructural changes in the synapses in the OPL, TEM was applied. At day 1, we observed many degenerated terminals that became very dark and contained several vacuoles (Figure 2C). Ribbons of photoreceptor terminals, which play a vital role in releasing synaptic vesicles, were floating in the cytoplasm of the photoreceptors (Figure 2D,E). At day 14 after light exposure, fine synapse structures were seldom seen in the OPL. The OPL was occupied by sponge-like structures (Figure 2F). The rod spherules were observed to retract into the ONL (Figure 2G,H).

Considering the relationship between the structural alterations and the functional consequences, we conducted western blotting to analyze the levels of PSD-95 and mGluR6 at different time points. Compared with the controls, PSD-95 declined continuously from 1 h after light exposure (Figure 3A). There was an obvious downregulation of mGluR6 at day 1; later, it remained at a relatively low level (Figure 3B). In

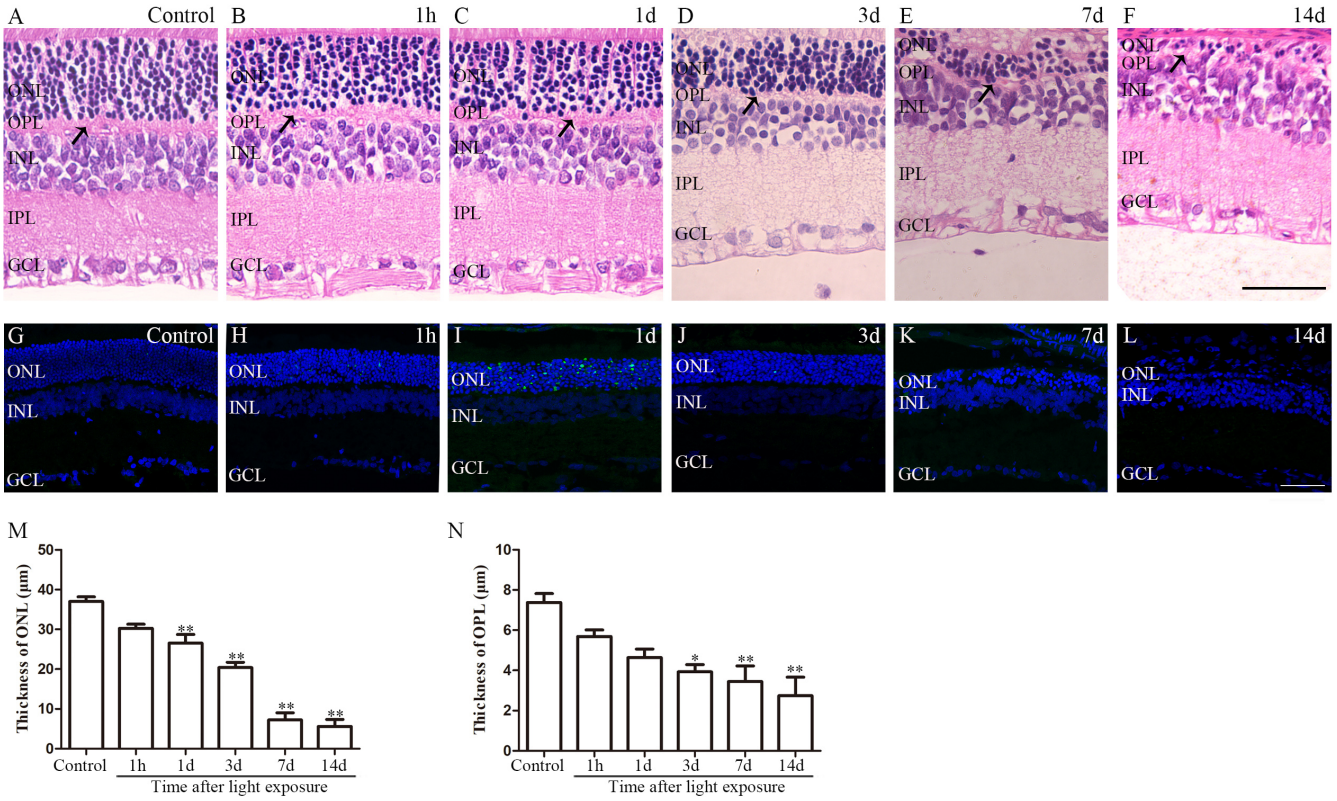

Figure 1. H&E and TUNEL staining of the retina. **A–F**: After light exposure, the number of photoreceptors decreases markedly. The thickness of the outer plexiform layer (OPL) also decreases gradually (arrow). **G**: In the control retina, positive staining is seldom observed. **H**: At 1 h after light exposure, positive cells start to appear in the outer nuclear layer (ONL). **I**: At day 1, the number of positive cells peaks. **J–L**: The number of positive cells gradually decreases. **M**: Quantification of the thickness of the ONL. n = 4. **p<0.01. **N**: Quantification of the thickness of OPL. n = 4. *p<0.05, **p<0.01. Scale bar: 50 μm.

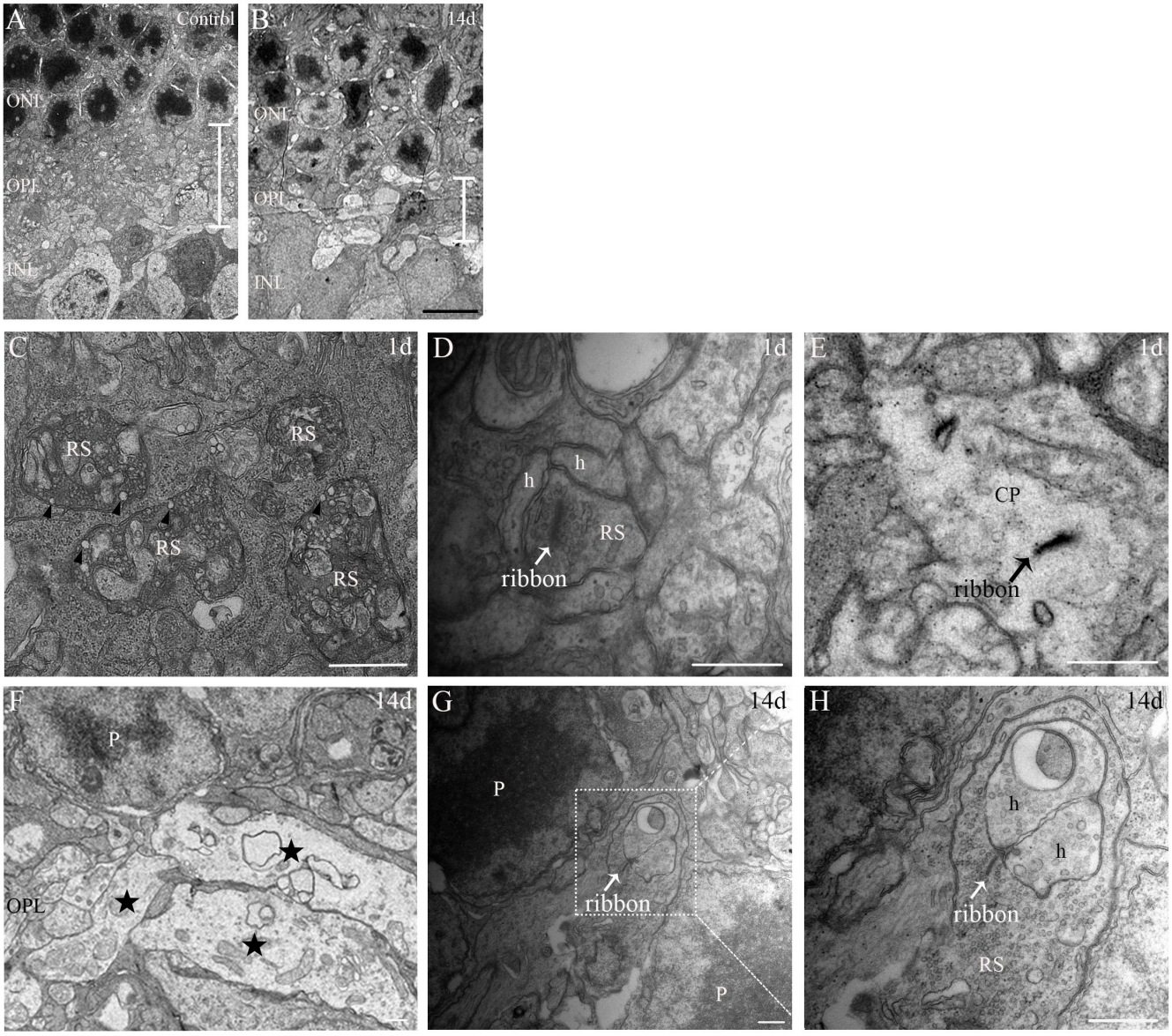

Figure 2. Transmission electron microscopy pictures of the retina show thinning of the OPL and degeneration of synapses in the OPL. **A**, **B**: The outer plexiform layer (OPL) is thinner in the light exposed animals at day 14 after light exposure than in the control animals. **C**: At day 1, many degenerated rod spherules (RSs) in the OPL have become very dark containing several vacuoles (arrowhead). **D**, **E**: At day 1, presynaptic ribbons float in the cytoplasm of the RSs and cone pedicle (arrow). **F**: At day 14, the OPL is occupied by a sponge-like structure (star). **G**: At day 14, the RSs are observed to retract into the outer nuclear layer (ONL; box). **H**: Magnification of the box area in **G**. CP, cone pedicle; h, horizontal cell; P, photoreceptor; RS, rod spherule. Scale bar: 5.0 µm for **A** and **B**, 0.5 µm for **C**–**H**.

the control animals (Figure 3C), labeling of mGluR6 showed strong punctate staining in the OPL. After light exposure, the staining of mGluR6 was diminished during the early course of the degeneration (Figure 3D–H). Downregulation of PSD-95 and mGluR6 indicated damage of pre- and postsynaptic components following degeneration of the photoreceptors.

Subsequent upregulation of proteins of the second synapses in the retina: As the upstream signal input had decreased gradually, we wondered whether other synaptic proteins of the interneurons had also been affected. Therefore, we evaluated specific synaptic proteins after light exposure. Compared with the controls, the protein levels of synapsin I in the degeneration group were upregulated continuously. At day 14, its levels were approximately twofold higher than that

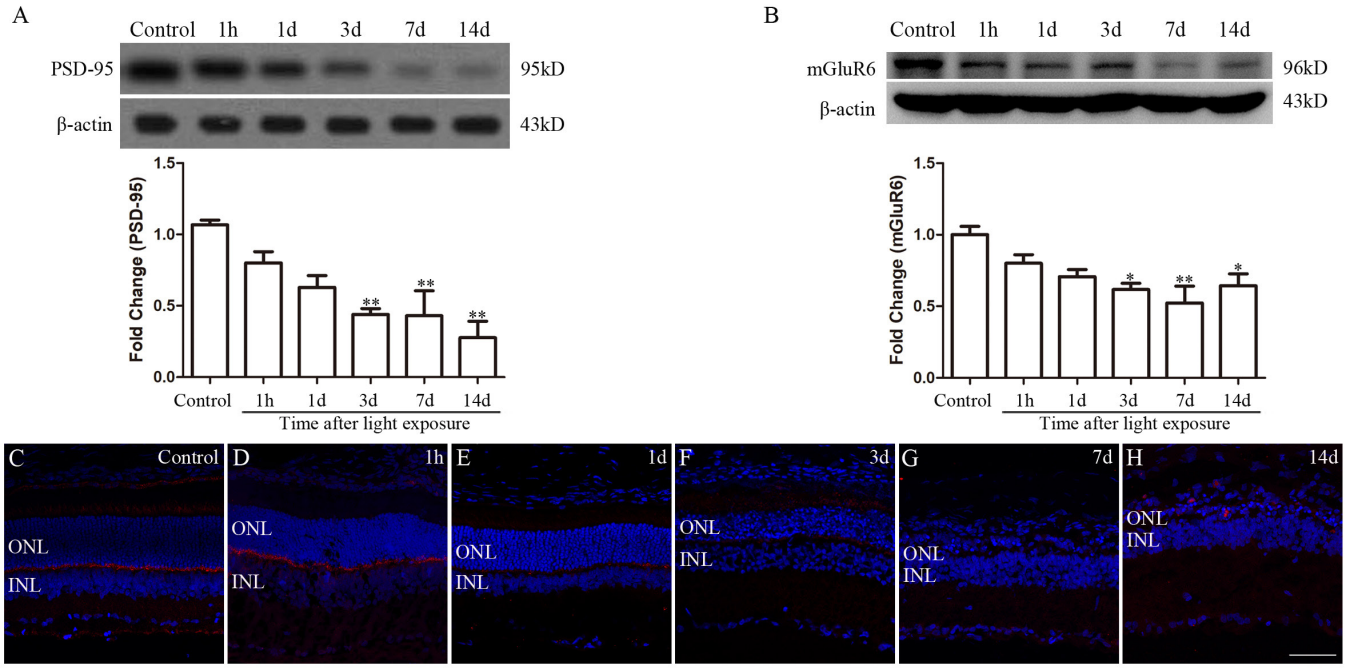

Figure 3. Analysis of synaptic proteins of first synapses in the retina. **A**: Western blotting of postsynaptic density-95 (PSD-95). **B**: Western blotting of metabotropic glutamate receptor 6 (mGluR6). n = 4. *p<0.05, **p<0.01. **C**: In the control animals, mGluR6 immunoreactivity is observed in the outer plexiform layer. **D–H**: After light exposure, the staining is diminished during the early course of the degeneration. Scale bar: 50 µm.

of the controls (2.11±0.47 and 1.04±0.26, respectively, p<0.05; Figure 4A). Unexpectedly, the protein levels of synaptophysin were unaltered even at day 14 when there were only a few layers of photoreceptors remaining (Figure 4A).

We performed immunofluorescence to clarify this result. In the control retinas, intense synaptophysin labeling was observed in the OPL and the IPL (Figure 4B). After light exposure, the intensity of the fluorescence in the OPL started to weaken, and the stripe appeared to become thinner (Figure 4C–F). At day 14, the staining was almost undetectable in the OPL (Figure 4G). Quantification of the staining intensity revealed that at day 14 the intensity of synaptophysin in the IPL was higher than that in the control retinas (p<0.01; Figure 4H).

Temporal and spatial relationships between microglia and synapses: Under the physiologic conditions of the fully developed retina, ramified microglia were observed in the inner retina, such as the ganglion cell layer, IPL, and the OPL (Figure 5A). Upon initiation of photoreceptor apoptosis induced by intense light, the microglia migrated toward the site of injury with simultaneous morphological changes. Their processes shortened, and their cell body became round (Figure 5B,C). During the degeneration, the population of microglia in the outer retina increased and peaked at day 3 (Figure 5D). As immunofluorescence against CD11b outlined the morphology of the activated microglia, we observed an interesting phenomenon. There were some microglia, with their nuclei located in the ONL, that terminated and stratified their processes in the OPL, which was made up of synaptic elements of the retina (Figure 5B,C).

To further explore the response of the microglia, we double immunostained the retina with antibodies against CD11b and PKC-α. PKC-α is a marker for rod bipolar cells, constituting the major population of the inner nuclear layer (INL) in rodent animals [18]. Double labeling revealed the tight interaction between microglial processes and dendrites of interneurons at 1 h after light exposure (Figure 6A). At day 3, this interaction could still be observed (Figure 6B). In some areas, both markers colocalized, as shown by the yellow color, implying close physical contact.

As the resolution of light microscopy is limited, we used TEM to gain insight into their spatial relationships. At day 1, microglia were found in the OPL (Figure 7A). Figure 7B shows the direct juxtaposition between microglia and synaptic elements at day 3. At day 14, although the OPL was filled with sponge-like structures, the microglia were found to have extended their processes among the structures (Figure 7C).

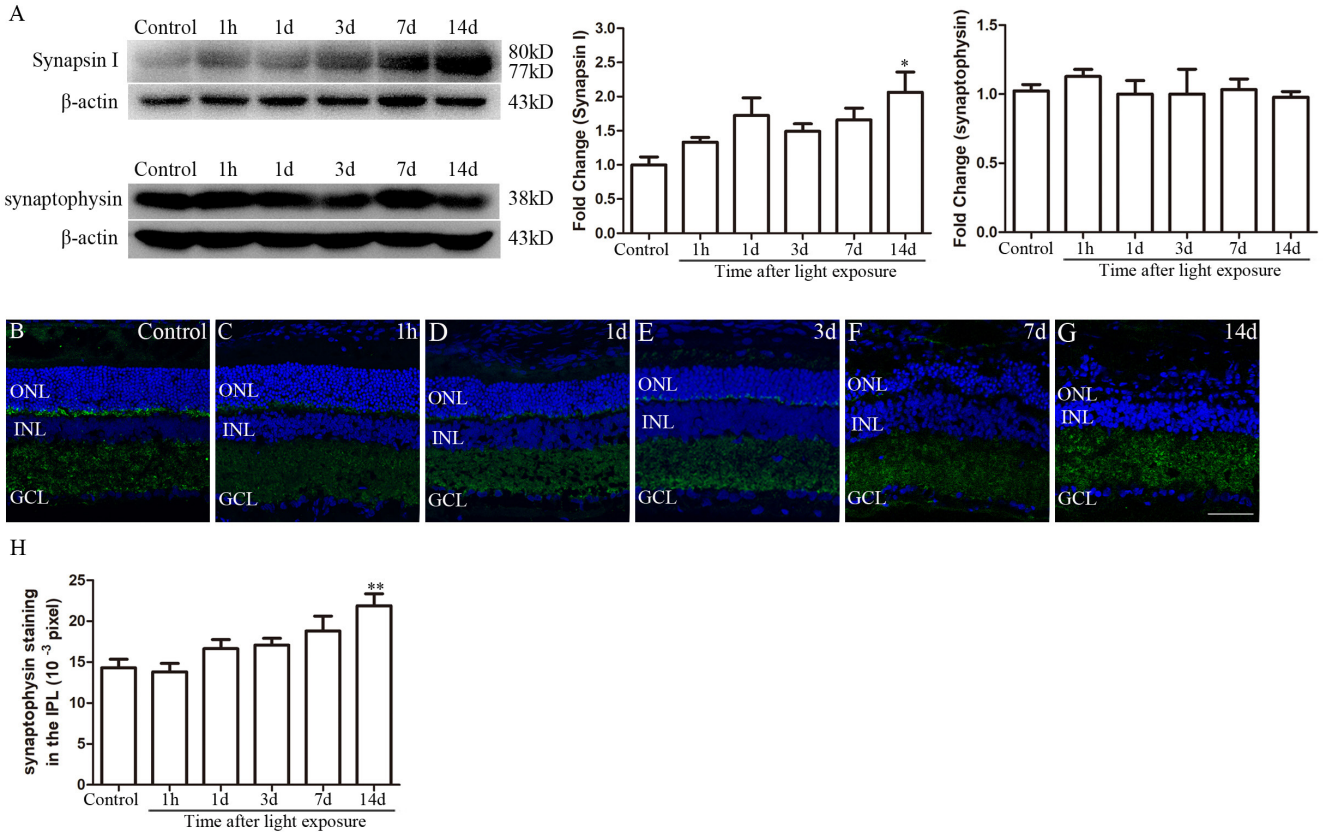

Figure 4. Analysis of synaptic proteins of the second synapses in the retina. **A**: Western blot of synapsin I and synaptophysin. n = 4. *p<0.05. **B**: In the control retina, intense labeling of synaptophysin is observed in the outer plexiform layer (OPL) and the inner plexiform layer (IPL). **C–F**: After light exposure, the intensity of the fluorescence of synaptophysin in the OPL starts to weaken. **G**: At day 14, the staining of synaptophysin is almost undetectable in the OPL. **H**: Quantification of the staining intensity of synaptophysin in the IPL. n = 6. **p<0.01. Scale bar: 50 µm.

Activated microglia directly engulf synaptic components: To explore whether the phagocytic activity of microglia in the OPL was enhanced, we double immunostained against CD11b and CD68, a marker of lysosomes. In the control retinas, CD68 signaling was seldom observed (Figure 8A). At day 3, there was upregulation of CD68 in the microglia in the OPL (Figure 8B).

As mGluR6, indirectly representing postsynaptic components, downregulated quickly after light exposure, we double immunostained the retinal slice 1 h after light exposure of mGluR6 and CD11b. Normally, staining of mGluR6 was observed in the OPL (Figure 9A). After light exposure, the punctate staining appeared elsewhere, colocalizing with CD11b (Figure 9B,C).

To directly illustrate whether microglia are phagocytosing synaptic components, IEM was performed. As shown in Figure 10A–C, in the control retinas, microglia having a thin ring of cytoplasm were observed in the inner part of the retina. PSD-95-immunoreactive electron-dense material was seldom seen inside the microglia in sections from the controls and the negative controls (without a primary antibody). A representative picture of the negative controls is shown in Figure 10D–F. At day 1 after light exposure, microglia were present in the OPL, and several 10 nm gold particles were observed inside the microglia (Figure 10G,H).

DISCUSSION

In the present study, we investigated structural and molecular alterations of synapses in a light-induced photoreceptor degeneration model and the possible role of activated microglia at the synapses. We characterized the destruction of the first synapses and the subsequent upregulation of the proteins of the second synapses in this model. We then observed microglial processes juxtaposed with synapse-associated elements in the OPL. Furthermore, we found that microglia engulfed synapses during light-induced degeneration.

As transfer of visual information starts at the synapses between photoreceptors and bipolar cells, their impairment affects vision directly. The present observation of OPL thinning and the ultrastructural abnormalities of synapses were similar to reports of other retinal degeneration models [19,20]. Darkened presynaptic components and floating ribbons were indicative of degenerating synapses. PSD-95 is a component of the submembrane cytoskeletal network in photoreceptor terminals [21]. In addition to PSD-95, which was evaluated in the present study, other synapse-associated proteins of photoreceptor terminals, such as bassoon, synaptophysin, and synaptic vesicle glycoprotein 2B, were found to be downregulated [22,23]. In other genetic retinal degeneration models, reduction of mGluR6 was found to be slower than in the present model [24,25]. Dunn reported that the loss of mGluR6 started as early as 2 h after photoreceptor ablation [26], and the rapid degeneration of the present model might explain this difference. The structural defects described above correlated strongly with the compromised synaptic function. As the b-wave of an electroretinogram reflects the

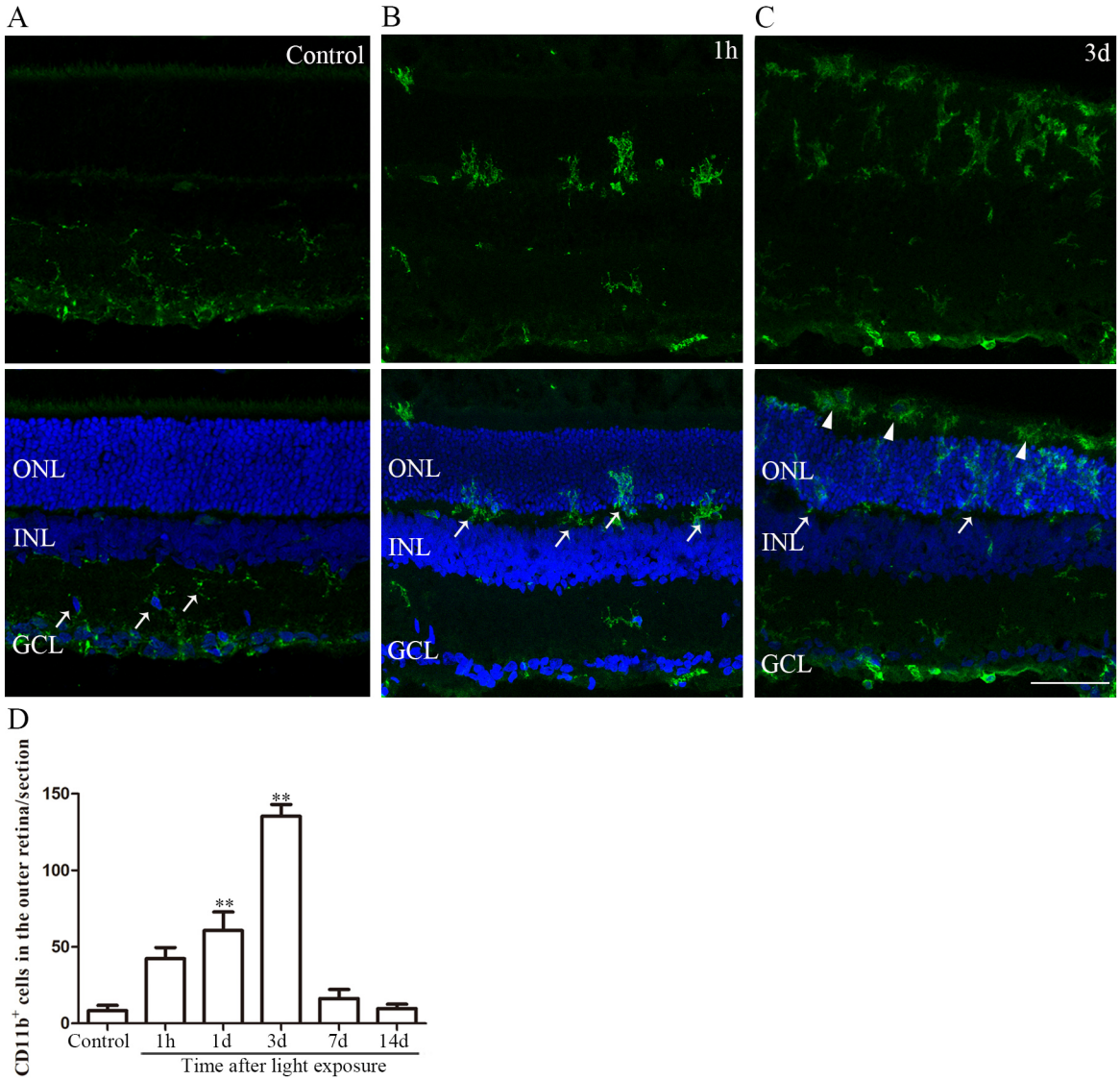

Figure 5. Immunofluorescence against CD11b after light exposure. **A**: In the control retinas, ramified microglia are observed (arrow). **B**: One hour after light exposure, activated microglia migrate toward the outer retina. In addition, some microglia terminate their processes in the outer plexiform layer (OPL; arrow). **C**: At day 3, some microglia are still terminating and stratifying their processes in the OPL (arrow). Some activated microglia are observed in the subretinal space (arrowhead). **D**: Quantification of the number of microglia in the outer retina (including the OPL, outer nuclear layer, and subretinal space) during retinal degeneration. n = 6. **p<0.01. Scale bar: 50 µm.

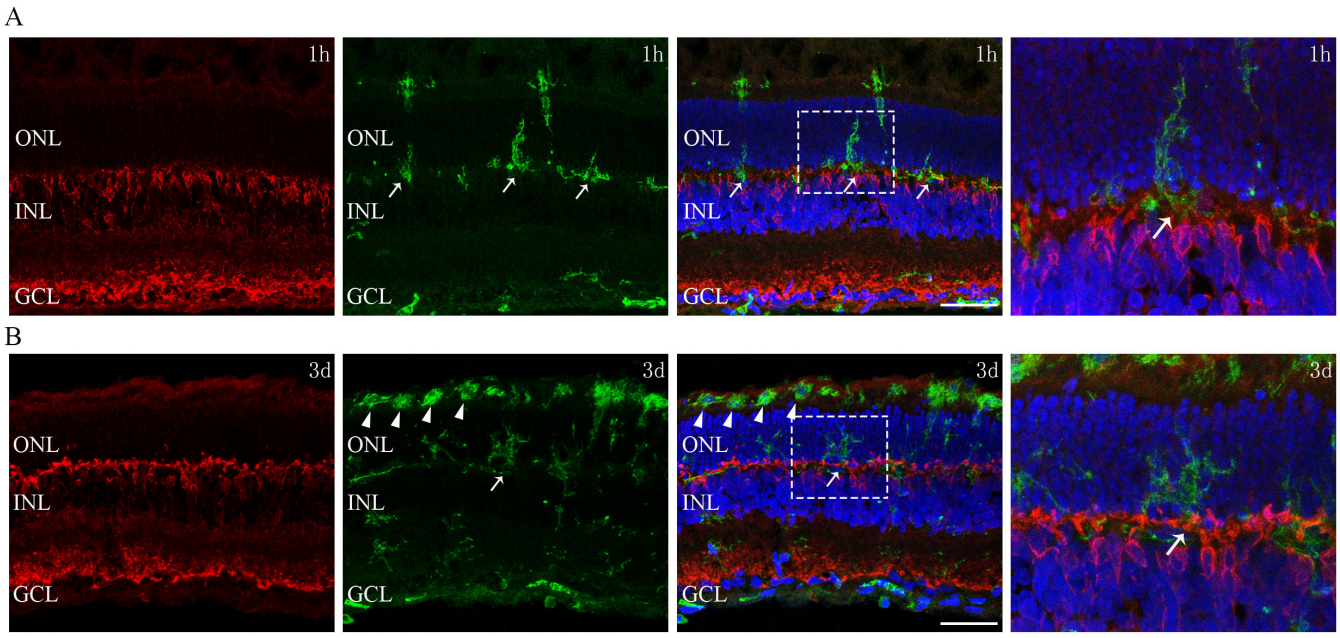

Figure 6. Double immunostaining against CD11b (green) and PKC-α (red). **A**: One hour after light exposure, tight interaction between microglial processes and dendrites of bipolar cells is observed (arrow). **B**: At day 3, some activated microglia are observed in the subretinal space (arrowhead), and tight interaction between microglia and bipolar cells can still be observed. Scale bar: 50 μm.

activity of the first synapses in the retina, prolonged implicit time and reduced amplitude are able to be recorded in retinal degeneration models and patients with retinitis pigmentosa (RP) [27-29]. Some researchers reported a much larger decrease in the b-wave compared with the decrease in the a-wave [30], which could not be fully explained by the death of the photoreceptors. This might demonstrate a dysfunction of the first synapses in the retina.

Microglia, representing an unusual population of cells among the mononuclear phagocytes, comprise the first line of defense of the CNS. Resting microglia display a form with ramified processes. Upon activation, the microglia undergo some stereotypic changes. The microglia's negative role in exacerbating neurodegenerative diseases of the CNS has been noted in research [31]. Our previous studies found that microglia indirectly contribute to the pathology of degeneration by producing proinflammatory mediators [32,33]. Recently, there is abundant evidence of the direct involvement of microglia in pathogenesis by engulfing synaptic materials. In an Alzheimer mouse model, Hong et al. observed

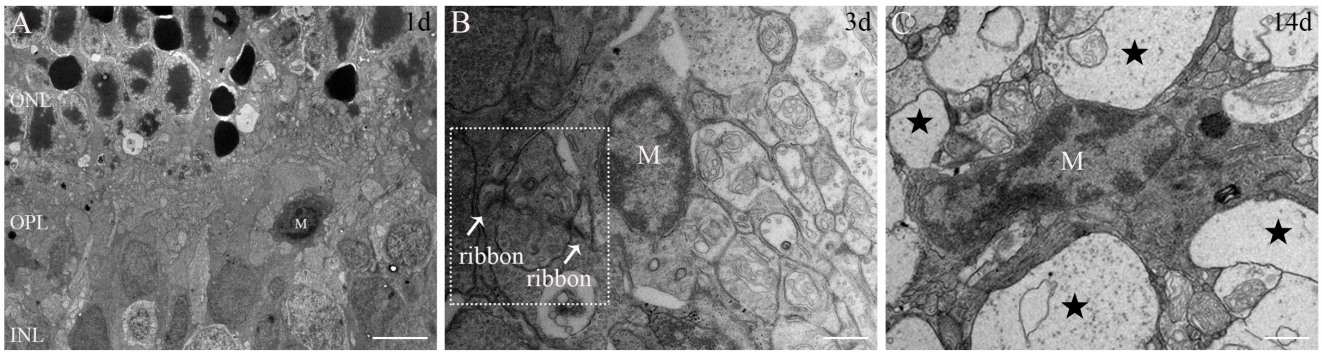

Figure 7. Transmission electron microscopy pictures shows a direct connection between the microglia and the synapses. **A**: At day 1, microglia are found in the outer plexiform layer (OPL). **B**: The direct juxtaposition between the microglia and synaptic elements (arrow) is observed at day 3 (box). **C**: At day 14, microglia are found to extend their processes between sponge-like structures (star) in the OPL. M, microglia. Scale bar: 5.0 μm for **A**, 0.5 μm for **B** and **C**.

that microglia engulfed synaptic elements when challenged with oligomeric amyloid-beta [34]. We found that activated microglia made direct connections with synaptic components in the OPL under light and electron microscopy levels. Upregulation of CD68 revealed the enhancement of phagocytosis of microglia. Engulfment of PSD-95 was confirmed with IEM. Paolicelli et al. reported that pre- and postsynaptic elements are a substrate for elimination by microglia [14]. Weinhard et al. confirmed phagocytosis of presynaptic material by microglia, but argued against elimination of postsynaptic material [35]. Unlike other synapses in the CNS where PSD-95 is located postsynaptically, it was found to be a part of presynaptic materials located in the terminals of photoreceptors in the retina [21]. In this study, we labeled mGluR6 to indirectly represent postsynaptic material. This study showed that engulfment of pre- and postsynaptic components may occur. A recent article reported that microglia mediate the synaptic material clearance of Royal College of Surgeons (RCS) rats [36]. However, the researchers observed phagocytosis by microglia only at the light microscopic level. No evidence of engulfment at the electron-microscopic level was available. Moreover, unlike in the case of the RCS rats, the light-induced photoreceptor degeneration model was a rapid degeneration model with a synchronized burst of apoptosis in the photoreceptors.

Regarding microglial processes in the OPL, there are two possibilities. One is that microglia in the ONL may extend their processes into the OPL on purpose. Researchers have revealed that molecules tagged to synapses and the surface receptors of microglia may mediate this connection [34,37]. The other possibility is that these processes just remain in their place while microglia in the OPL start to move toward the outer retina. Regardless, the functional state of these processes was different from normal, as the phagocytosis of microglia was enhanced. Dynamic continuous observation in vivo is required to solve this problem.

The engulfment of synapses by microglia observed in the present study may impair the synapses and contribute to the pathology of retinal degeneration. There was also the possibility that it served to remove the debris of dead cells and limit the progression of the disease. Equally, it is possible that the effect was harmful or beneficial at different stages. However, intense blue light initiated the death of photoreceptors. There was little evidence to show the death of bipolar cells in this model, but we found receptors expressed by bipolar cells inside microglia. Drawing on the emerging studies that have revealed the effects of microglia on synapses, we are inclined to believe that microglia play a role or a partial role in synaptic impairment, rather than just being battlefield cleaners. To fully elucidate the effect of the engulfment of synapses by microglia, inhibition experiments should be performed in the future.

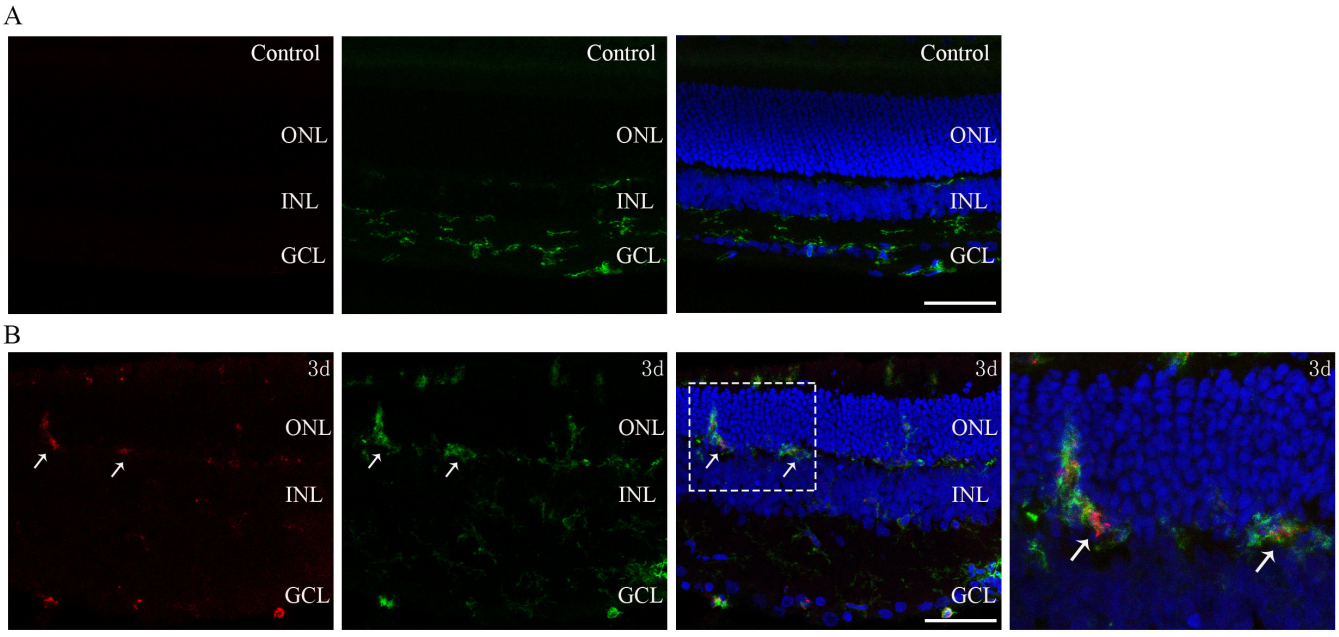

Figure 8. Double immunostaining against CD11b (green) and CD68 (red). **A**: In the control retinas, CD68 signaling is seldom observed. **B**: At day 3, there is upregulation of CD68 in microglia in the outer plexiform layer (OPL) after light exposure (arrow). Scale bar: 50 µm.

Synaptic impairment might precede the loss of neurons in the CNS [38,39]. Researchers have also reported that the protein levels of some synaptic proteins are downregulated before there is a detectable loss of neurons in an RP model and a diabetic retinopathy model [7,40]. Because synapses are highly sophisticated structures, their molecular composition is tightly associated with their function. The degeneration of photoreceptors in this model was induced by blue light which might start as early as the process of light exposure. Therefore, it was difficult to evaluate the impairment of synapses at the initial phase in this model. It surely warrants further study.

Previous studies have reported compensatory changes in synaptic proteins in bipolar cells and amacrine cells after the loss of photoreceptors [41,42]. Synapsin I, a synaptic vesicle-associated protein, is necessary for clustering the synaptic vesicles. It is expressed selectively by amacrine cells in the retina [43]. Synaptophysin, a synaptic vesicle glycoprotein, plays a significant role in releasing neurotransmitter vesicles of neurons, including photoreceptors and bipolar cells [44]. We have also shown in biochemical and immunofluorescent analyses that these proteins associated with the synaptic function of second synapses in the retina are upregulated during disease progression. This may account for the spontaneous bursts of spikes in retinal ganglion cells [45].

In summary, this study showed that there are early synaptic impairment and late compensatory changes in the downstream synapses in this photic injury model. Activated microglia touched and directly engulfed synaptic materials. Microglia may play a role or a partial role in synaptic changes.

APPENDIX 1. MEASUREMENT OF THE MEAN OPTICAL DENSITY IN IMMUNOFLUORESCENCE USING IMAGEJ

To access the data, click or select the words "Appendix 1."

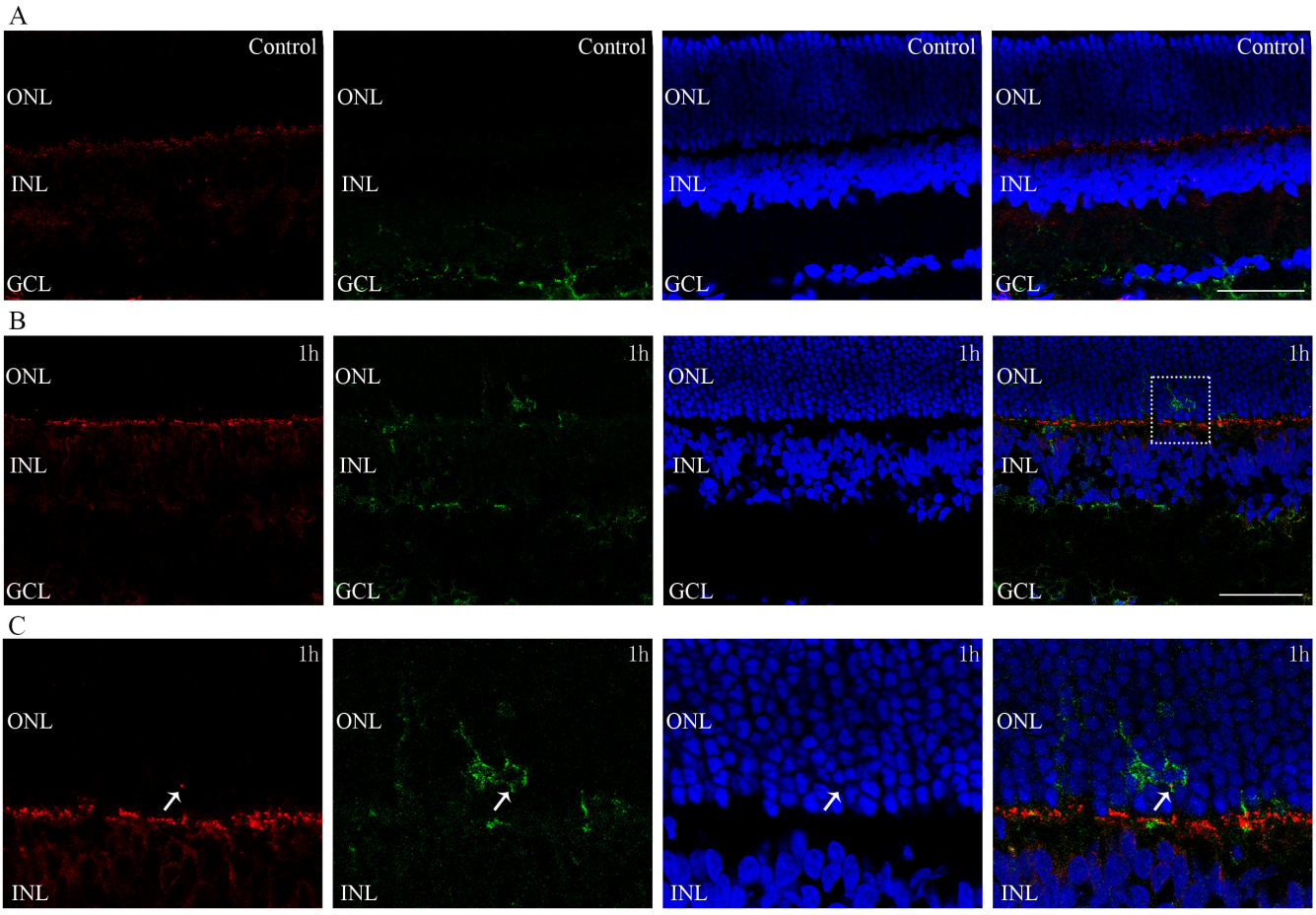

Figure 9. Double immunostaining against CD11b (green) and mGluR6 (red). **A**: In the control animals, metabotropic glutamate receptor 6 (mGluR6) immunoreactivity is observed in the outer plexiform layer. **B**: One hour after light exposure, punctate staining of mGluR6 appears elsewhere, colocalizing with CD11b (arrow). **C**: Magnification of the box area in **B**. Scale bar: 50 µm.

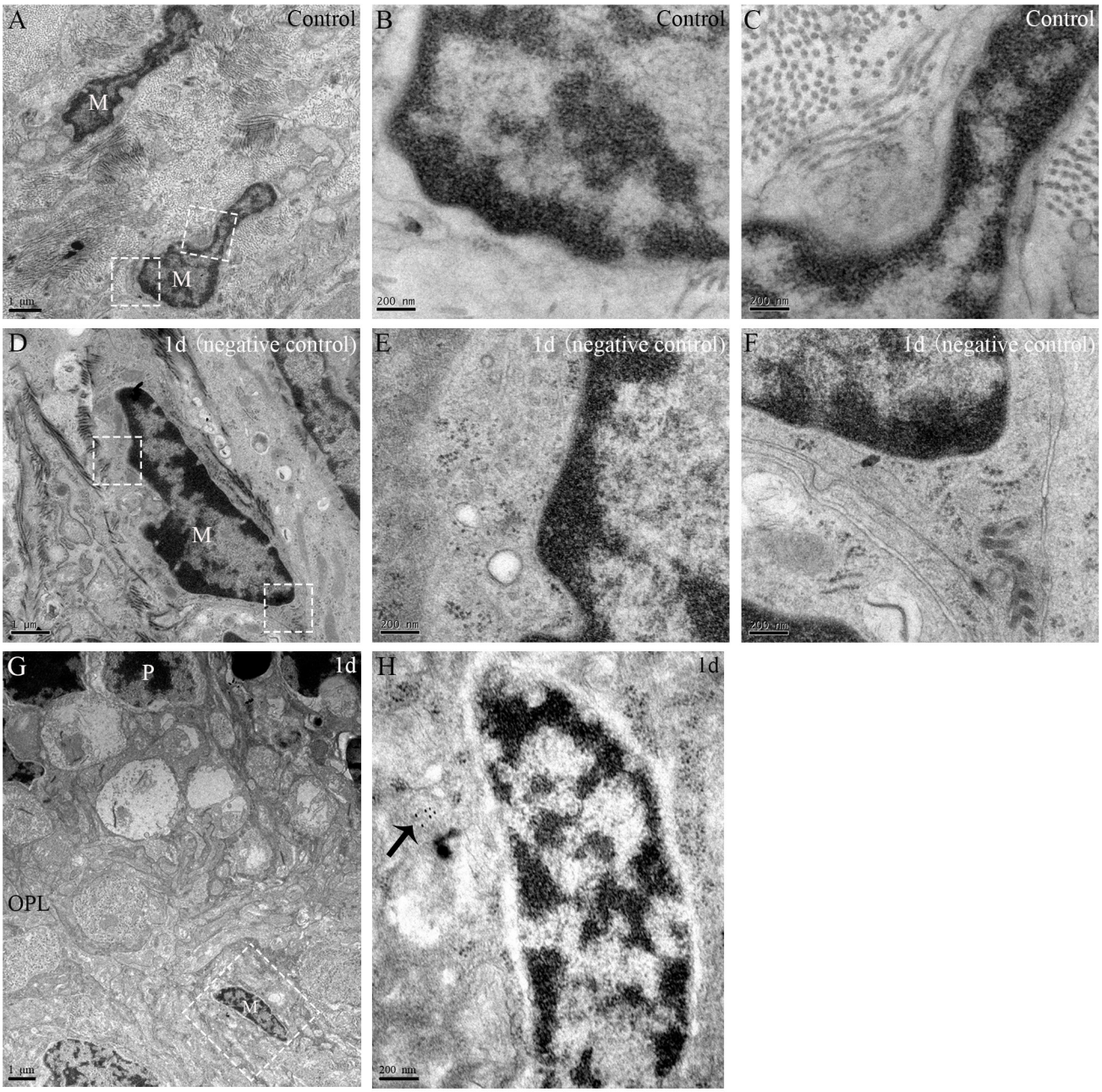

Figure 10. Immunoelectron microscopy shows engulfment of synaptic material by the microglia. **A**: In the control animals, microglia are observed in the inner part of the retina. Postsynaptic density-95 (PSD-95)-immunoreactive electron-dense material is seldom seen inside the microglia. **B, C**: Magnification of the box area in **A**. No PSD-95-immunoreactive electron-dense material is observed in the cytoplasm of the microglia. **D**: A representative picture of a negative control at day 1 (without primary antibody). **E, F**: Magnification of the box area in **D**. No PSD-95-immunoreactive electron-dense material is observed in the cytoplasm of the microglia. **G, H**: At day 1, microglia are occasionally presented in the outer plexiform layer (OPL), and several 10 nm gold particles are observed inside the microglia (arrow). **H**: Magnification of the box area in **G**. M, microglia; P, photoreceptor.

ACKNOWLEDGMENTS

This work was supported by research grants from the National Natural Science Foundation of China (No.81570855 and No.81570854), the National Natural Science Foundation for Young Scholar of China (No.81500723) and the National Key Basic Research Program of China (2013CB967503). We are grateful to co-corresponding author Gezhi Xu (xugezhi@sohu.com) from Department of Ophthalmology, Shanghai Key Laboratory of Visual Impairment and Restoration, Eye & ENT Hospital, Fudan University. Disclosure: S. Xu, None; P. Zhang, None; M. Zhang, None; X. Wang, None; G. Li, None; G. Xu, None; Y. Ni, None

REFERENCES

1. Wert KJ, Lin J. SH T. General pathophysiology in retinal degeneration. Dev Ophthalmol 2014; 53:33-43. [PMID: 24732759].
2. Marigo V. Programmed cell death in retinal degeneration: targeting apoptosis in photoreceptors as potential therapy for retinal degeneration. Cell Cycle 2007; 6:652-5. [PMID: 17374995].
3. Santos A, Humayun MS, de Juan E Jr, Greenburg RJ, Marsh MJ, Klock IB, Milam AH. Preservation of the inner retina in retinitis pigmentosa: a morphometric analysis. Arch Ophthalmol 1997; 115:511-5. [PMID: 9109761].
4. Nagar S, Krishnamoorthy V, Cherukuri P, Jain V, Dhingra NK. Early remodeling in an inducible animal model of retinal degeneration. Neuroscience 2009; 160:517-29. [PMID: 19272416].
5. Beier C, Hovhannisyan A, Weiser S, Kung J, Lee S, Lee DY, Huie P, Dalal R, Palanker D, Sher A. Deafferented adult rod bipolar cells create new synapses with photoreceptors to restore vision. J Neurosci 2017; 37:4635-44. [PMID: 28373392].
6. Stephan AH, Barres BA, Stevens B. The complement system: an unexpected role in synaptic pruning during development and disease. Annu Rev Neurosci 2012; 35:369-89. [PMID: 22715882].
7. Roche SL, Wyse-Jackson AC, Byrne AM, Ruiz-Lopez AM, Cotter TG. Alterations to retinal architecture prior to photoreceptor loss in a mouse model of retinitis pigmentosa. Int J Dev Biol 2016; 60:127-39. [PMID: 27160072].
8. Petralia RS, Wang Y, Mattson MP, Yao PJ. Invaginating presynaptic terminals in neuromuscular junctions, photoreceptor terminals, and other synapses of animals. Neuromolecular Med 2017; 19:193-240. [PMID: 28612182].
9. Reh TA. Photoreceptor transplantation in late stage retinal degeneration. Invest Ophthalmol Vis Sci 2016; 57:ORSFg1-7. [PMID: 27116664].
10. Light JG, Fransen JW, Adekunle AN, Adkins A, Pangeni G, Loudin J, Mathieson K, Palanker DV, McCall MA, Pardue MT. Inner retinal preservation in rat models of retinal degeneration implanted with subretinal photovoltaic arrays. Exp Eye Res 2014; 128:34-42. [PMID: 25224340].
11. Kreutzberg GW. Microglia: a sensor for pathological events in the CNS. Trends Neurosci 1996; 19:312-8. [PMID: 8843599].
12. Wake H, Moorhouse AJ, Jinno S, Kohsaka S, Nabekura J. Resting microglia directly monitor the functional state of synapses *in vivo* and determine the fate of ischemic terminals. J Neurosci 2009; 29:3974-80. [PMID: 19339593].
13. Schafer DP, Lehrman EK, Kautzman AG, Koyama R, Mardinly AR, Yamasaki R, Ransohoff RM, Greenberg ME, Barres BA, Stevens B. Microglia sculpt postnatal neural circuits in an activity and complement-dependent manner. Neuron 2012; 74:691-705. [PMID: 22632727].
14. Paolicelli RC, Bolasco G, Pagani F, Maggi L, Scianni M, Panzanelli P, Giustetto M, Ferreira TA, Guiducci E, Dumas L, Ragozzino D, Gross CT. Synaptic pruning by microglia is necessary for normal brain development. Science 2011; 333:1456-8. [PMID: 21778362].
15. Wang X, Zhao L, Zhang J, Fariss RN, Ma W, Kretschmer F, Wang M, Qian HH, Badea TC, Diamond JS, Gan W, Roger JE, Wong WT. Requirement for microglia for the maintenance of synaptic function and integrity in the mature retina. J Neurosci 2016; 36:2827-42. [PMID: 26937019].
16. Rajendran L, Paolicelli RC. Microglia-mediated synapse loss in Alzheimer's disease. J Neurosci 2018; 38:2911-9. [PMID: 29563239].
17. Aono H, Choudhury ME, Higaki H, Miyanishi K, Kigami Y, Fujita K, Akiyama J, Takahashi H, Yano H, Kubo M, Nishikawa N, Nomoto M, Tanaka J. Microglia may compensate for dopaminergic neuron loss in experimental Parkinsonism through selective elimination of glutamatergic synapses from the subthalamic nucleus. Glia 2017; 65:1833-47. [PMID: 28836295].
18. Ruether K, Feigenspan A, Pirngruber J, Leitges M, Baehr W, Strauss O. PKCα is essential for the proper activation and termination of rod bipolar cell response. Invest Ophthalmol Vis Sci 2010; 51:6051-8. [PMID: 20554612].
19. Takada Y, Vijayasarathy C, Zeng Y, Kjellstrom S, Bush RA, Sieving PA. Synaptic pathology in retinoschisis knockout (*Rs1*$^{-/y}$) mouse retina and modification by rAAV-*Rs1* gene delivery. Invest Ophthalmol Vis Sci 2008; 49:3677-86. [PMID: 18660429].
20. Zhang J, Tuo J, Cao X, Shen D, Li W, Chan C. Early degeneration of photoreceptor synapse in Ccl2/Cx3cr1-deficient mice on Crb1^{rd8} background. Synapse 2013; 67:515-31. [PMID: 23592324].
21. Koulen P, Fletcher EL, Craven SE, Bredt DS, Wassle H. Immunocytochemical localization of the postsynaptic density protein PSD-95 in the mammalian retina. J Neurosci 1998; 18:10136-49. [PMID: 9822767].
22. Fariss RN, Li Z, Milam AH. Abnormalities in rod photoreceptors, amacrine cells, and horizontal cells in human retinas with retinitis pigmentosa. Am J Ophthalmol 2000; 129:215-23. [PMID: 10682975].

23. Lu B, Morgans CW, Girman S, Lund R, Wang S. Retinal morphological and functional changes in an animal model of retinitis pigmentosa. Vis Neurosci 2013; 30:77-89. [PMID: 23510618].

24. Barhoum R, Martínez-Navarrete G, Corrochano S, Germain F, Fernandez-Sanchez L, de la Rosa EJ, de la Villa P, Cuenca N. Functional and structural modifications during retinal degeneration in the rd10 mouse. Neuroscience 2008; 155:698-713. [PMID: 18639614].

25. Singh RK, Kolandaivelu S, Ramamurthy V. Early alteration of retinal neurons in Aipl1$^{-/-}$ animals. Invest Ophthalmol Vis Sci 2014; 55:3081-92. [PMID: 24736053].

26. Dunn FA. Photoreceptor ablation initiates the immediate loss of glutamate receptors in postsynaptic bipolar cells in retina. J Neurosci 2015; 35:2423-31. [PMID: 25673837].

27. Ueno S, Koyasu T, Kominami T, Sakai T, Kondo M, Yasuda S, Terasaki H. Focal cone ERGs of rhodopsin Pro347Leu transgenic rabbits. Vision Res 2013; 91:118-23. [PMID: 23973440].

28. Cuenca N, Fernández-Sánchez L, Campello L, Maneu V, De la Villa P, Lax P, Pinilla I. Cellular responses following retinal injuries and therapeutic approaches for neurodegenerative diseases. Prog Retin Eye Res 2014; 43:17-75. [PMID: 25038518].

29. Ebdali S, Hashemi B, Hashemi H, Jafarzadehpur E, Asgari S. Time and frequency components of ERG responses in retinitis pigmentosa. Int Ophthalmol 2018; 38:2435-44. [PMID: 29189947].

30. Strettoi E, Porciatti V, Falsini B, Pignatelli V, Rossi C. Morphological and functional abnormalities in the inner retina of the rd/rd mouse. J Neurosci 2002; 22:5492-504. [PMID: 12097501].

31. Spangenberg EE, Lee RJ, Najafi AR, Rice RA, Elmore MRP, Blurton-Jones M, West BL, Green KN. Eliminating microglia in Alzheimer's mice prevents neuronal loss without modulating amyloid-β pathology. Brain 2016; 139:1265-81. [PMID: 26921617].

32. Ni YQ, Xu GZ, Hu WZ, Shi L, Qin YW, Da CD. Neuroprotective effects of naloxone against light-induced photoreceptor degeneration through inhibiting retinal microglial activation. Invest Ophthalmol Vis Sci 2008; 49:2589-98. [PMID: 18515588].

33. Zhang M, Xu G, Liu W, Ni Y, Zhou W. Role of fractalkine/CX3CR1 interaction in light-induced photoreceptor degeneration through regulating retinal microglial activation and migration. PLoS One 2012; 7:e35446-[PMID: 22536384].

34. Hong S, Beja-Glasser VF, Nfonoyim BM, Frouin A, Li S, Ramakrishnan S, Merry KM, Shi Q, Rosenthal A, Barres BA, Lemere CA, Selkoe DJ, Stevens B. Complement and microglia mediate early synapse loss in Alzheimer mouse models. Science 2016; 352:712-6. [PMID: 27033548].

35. Weinhard L, di Bartolomei G, Bolasco G, Machado P, Schieber NL, Neniskyte U, Exiga M, Vadisiute A, Raggioli A, Schertel A, Schwab Y, Gross CT. Microglia remodel synapses by presynaptic trogocytosis and spine head filopodia induction. Nat Commun 2018; 9:1228-[PMID: 29581545].

36. He J, Zhao C, Dai J, Weng CH, Bian BSJ, Gong Y, Ge L, Fang Y, Liu H, Xu H, Yin ZQ. Microglia mediate synaptic material clearance at the early stage of rats with retinitis pigmentosa. Front Immunol 2019; 10:912-[PMID: 31105708].

37. Hoshiko M, Arnoux I, Avignone E, Yamamoto N, Audinat E. Deficiency of the microglial receptor CX3CR1 impairs postnatal functional development of thalamocortical synapses in the barrel cortex. J Neurosci 2012; 32:15106-11. [PMID: 23100431].

38. Bai Y, Li M, Zhou Y, Ma L, Qiao Q, Hu W, Li W, Wills ZP, Gan W. Abnormal dendritic calcium activity and synaptic depotentiation occur early in a mouse model of Alzheimer's disease. Mol Neurodegener 2017; 12:86-[PMID: 29137651].

39. Kovalenko M, Milnerwood A, Giordano J, St. Claire J, Guide JR, Stromberg M, Gillis T, Sapp E, DiFiglia M, MacDonald ME, Carroll JB, Lee J, Tappan S, Raymond L, Wheeler VC. Htt$^{Q111/+}$ Huntington's disease knock-in mice exhibit brain region-specific morphological changes and synaptic dysfunction. J Huntingtons Dis 2018; 7:17-33. [PMID: 29480209].

40. VanGuilder HD, Brucklacher RM, Patel K, Ellis RW, Freeman WM, Barber AJ. Diabetes downregulates presynaptic proteins and reduces basal synapsin I phosphorylation in rat retina. Eur J Neurosci 2008; 28:1-11. [PMID: 18662330].

41. Montalban-Soler L, Alarcon-Martinez L, Jimenez-Lopez M, Salinas-Navarro M, Galindo-Romero C, Bezerra DSF, Garcia-Ayuso D, Aviles-Trigueros M, Vidal-Sanz M, Agudo-Barriuso M, Villegas-Perez MP. Retinal compensatory changes after light damage in albino mice. Mol Vis 2012; 18:675-93. [PMID: 22509098].

42. Dagar S, Nagar S, Goel M, Cherukuri P, Dhingra N. Loss of photoreceptors results in upregulation of synaptic proteins in bipolar cells and amacrine cells. PLoS One 2014; 9:e90210-50. [PMID: 24595229].

43. Mandell JW, Czernik AJ, De Camilli P, Greengard P, Townes-Anderson E. Differential expression of synapsins I and II among rat retinal synapses. J Neurosci 1992; 12:1736-49. [PMID: 1578266].

44. Brandstätter JH, Löhrke S, Morgans CW, Wässle H. Distributions of two homologous synaptic vesicle proteins, synaptoporin and synaptophysin, in the mammalian retina. J Comp Neurol 1996; 370:1-10. [PMID: 8797152].

45. Margolis DJ, Detwiler PB. Cellular origin of spontaneous ganglion cell spike activity in animal models of retinitis pigmentosa. J Ophthalmol 2011; 2011:1-6. [PMID: 20936060].

Articles are provided courtesy of Emory University and the Zhongshan Ophthalmic Center, Sun Yat-sen University, P.R. China. The print version of this article was created on 1 May 2021. This reflects all typographical corrections and errata to the article through that date. Details of any changes may be found in the online version of the article.